Effects of Lipid Interactions on Model Vesicle Engulfment by Alveolar Macrophages

Matthew J. Justice,[†‡] Daniela N. Petrusca,[‡] Adriana L. Rogozea,[†‡] Justin A. Williams,[†] Kelly S. Schweitzer,[‡] Irina Petrache,[‡§] Stephen R. Wassall,[†] and Horia I. Petrache[†*]

[†]Department of Physics, Indiana University Purdue University Indianapolis, Indianapolis, Indiana; [‡]Department of Medicine, Indiana University School of Medicine, Indianapolis, Indiana; and [§]Department of Medicine, Richard L. Roudebush Veterans' Affairs Medical Center, Indianapolis, Indiana

ABSTRACT The engulfment function of macrophages relies on complex molecular interactions involving both lipids and proteins. In particular, the clearance of apoptotic bodies (efferocytosis) is enabled by externalization on the cell target of phosphatidylserine lipids, which activate receptors on macrophages, suggesting that (local) specific lipid-protein interactions are required at least for the initiation of efferocytosis. However, in addition to apoptotic cells, macrophages can engulf foreign bodies that vary substantially in size from a few nanometers to microns, suggesting that nonspecific interactions over a wide range of length scales could be relevant. Here, we use model lipid membranes (made of phosphatidylcholine, phosphatidylserine, and ceramide) and rat alveolar macrophages to show how lipid bilayer properties probed by small-angle x-ray scattering and solid-state ^{2}H NMR correlate with engulfment rates measured by flow cytometry. We find that engulfment of protein-free model lipid vesicles is promoted by the presence of phosphatidylserine lipids but inhibited by ceramide, in accord with a previous study of apoptotic cells. We conclude that the roles of phosphatidylserine and ceramide in phagocytosis is based, at least in part, on lipid-mediated modification of membrane physical properties, including interactions at large length scales as well as local lipid ordering and possible domain formation.

INTRODUCTION

Macrophages are white blood cells (leukocytes) on the order of 10 μm in diameter that can engulf and digest cellular material and harmful contaminants in a process called phagocytosis (1,2). In addition to this defensive role, macrophages also recycle cellular material resulting from apoptotic (dying) cells by a similar, but target-specific, process of engulfment and digestion called efferocytosis. Macrophages can ingest particles of 10 μm or more in diameter through a mechanism involving internal membrane reserves that are needed to accommodate changes in macrophage shape and volume (3).

To perform their efferocytosis function properly, macrophages must be selective to discriminate between live and dead cells. A current explanation for this selectivity in efferocytosis involves the recognition of phosphatidylserine (PS) lipids that are externalized by the plasma membranes of apoptotic cells (4,5). Recognition of PS lipids by macrophages and proper clearance of apoptotic cells are crucial for homeostatic disposal of cellular corpses, a process that inhibits inflammation. If efferocytosis is defective, apoptotic cell contents are spilled, triggering local inflammatory responses that further activate macrophages and exacerbate inflammation (6). In addition to PS-induced activation, mechanical stimulation or contact with glass coverslips is also sufficient to activate macrophages (3). These observations indicate that macrophage activation and the mechanics of subsequent engulfment could depend on the physical properties of lipid membranes.

Membrane properties are a consequence of lipid-lipid interactions, which are manifested over a broad range of length scales (7,8). At molecular scales (1–10 nm), lipid interactions determine molecular packing within membranes, characterized by structural parameters accessible by small-angle x-ray scattering (SAXS) (9,10) and by lipid order parameters obtained from solid-state NMR spectroscopy (10,11). The exact molecular packing within lipid bilayers is determined by the balance of forces between hydrophilic headgroups and hydrophobic chains, with the lipid headgroup having a dominant role in the case of saturated and monounsaturated acyl chains (10,12,13). For example, PS lipids pack >10% more tightly within lipid membranes than do the neutral (zwitterionic) phosphatidylcholine (PC) lipids for the same acyl chain composition, thus creating more rigid membranes (10). This effect is seen by both x-ray measurements of area/lipid as well as by solid-state ^{2}H NMR measurements of hydrocarbon chain order parameters (10,12). At larger length scales on the order of cellular size (0.1–10 μm; mesoscopic regime), lipid interactions give rise to attractive and repulsive forces between neighboring membranes (14–17). At this scale, membrane interactions are manifested through their three main contributions: van der Waals, electrostatics, and entropic terms associated with lipid hydration and with membrane undulations (10,14,18–20). Since PS lipids carry net negative charge, the balance between electrostatics and all other membrane interactions is expected to play a major role in

Submitted July 16, 2013, and accepted for publication December 23, 2013.

*Correspondence: hpetrach@iupui.edu

Editor: Klaus Gawrisch.

0006-3495/14/02/0598/12 $2.00

http://dx.doi.org/10.1016/j.bpj.2013.12.036

efferocytosis that necessarily involves intermembrane interactions.

The van der Waals interaction between lipid membranes arises from charge fluctuations (electric polarization) and it causes neighboring membranes to attract each other (16,21). This is the reason lipid bilayers made of PC lipids form multilamellar vesicles (MLVs). MLVs are closed structures typically composed of 10^2–10^4 lipid bilayers, separated by aqueous layers, stacked regularly with a repeat spacing (*D*-spacing) on the order of 60 Å (14). When inspected by x-ray scattering, MLVs produce scattering rings from which *D*-spacings can be measured (18). Size-wise, MLVs made of PC lipids range from 10 nm to 10 μm, depending on sample preparation and history. PS lipids can also form MLVs, depending on their acyl chain composition (22), as well as ionic strength and pH (23,24). Unsaturated PS lipids, such as dioleoylphosphatidylserine (DOPS), at low ionic strength have been shown to form disordered structures (25) including unilamellar vesicles (ULVs), unless they are subjected to dehydration or osmotic stress (10). Due to electrostatic repulsion, adding PS lipids to PC bilayers is expected to cause a transition from MLVs to disordered structures at a particular PS/PC ratio. Since membrane interactions are highly sensitive to sample composition (15,26,27), the exact transition point is expected to depend on a number of factors, including ionic strength (17), pH, and the presence of additional molecular species in the PS/PC mixtures.

In this work, we investigate how physical properties of model PS/PC lipid vesicles correlate with their engulfment by alveolar macrophages (AMs). AMs are specialized macrophages stationed in pulmonary alveoli that are essential to clearing the lungs of dust and microorganisms, in addition to clearing apoptotic cells (28–31). It was recently shown that the AM efferocytosis function is affected by ceramide (Cer). Specifically, it was shown that Cers reduce efferocytosis of apoptotic cells in vivo (in rat lungs) and ex vivo in cultured primary human and murine AMs (32). Cers are a family of sphingolipids with both structural and signaling roles (33). The most notable structural roles of Cers are in the lipid composition of skin (34–36), while the Cer species composition of AMs and their extracellular milieu was recently described (32). As signaling molecules, Cers are involved in a number of cellular processes, including cellular differentiation (37), senescence (38), apoptosis (39,40), and possibly cell migration (41). Cer species vary according to their fatty acid chain length and saturation, with chains of $>$18 carbons found primarily in the skin stratum corneum (42,43). Added to lipid bilayers, ceramides can affect the gel-to-fluid and lamellar-to-hexagonal phase transitions when mixed with saturated phospholipids (44–46), phosphatidylethanolamine headgroups (47), or N-palmitoylsphingomyelin (48). However, when added to unsaturated palmitoyloleoylphosphatidylcholine (POPC) lipid, which has a lower melting temperature than saturated lipids, no phase change is detected for a broad range of temperatures (46,49). When performing signaling roles, Cer with various chain lengths can be recruited into cholesterol-rich areas of the plasma membrane that serve as the platform for signaling proteins (50,51). It has been shown that these patches, called lipid rafts, are important in cell signaling (52), including that triggered by Cers (53).

In a cell culture model of apoptotic cell engulfment using alveolar macrophages and ultraviolet-irradiated lymphocyte targets (32), preincubation of macrophages with Cers was shown to markedly decrease their engulfment efficiency. This indicates that Cer affects either the macrophage signaling processes (and recognition of PS) or the subsequent fusion between plasma membranes, or both. Because of this role of Cer in lipid interactions, in this work we study model lipid vesicles and macrophages with and without added Cer. We measured the combined effect of PS lipids and Cer (see Fig. 1 for chemical structures) on the physical structure of PC membranes using solid-state ^{2}H NMR spectroscopy (54), an experimental method that gives detailed information on molecular organization within lipid bilayers. This powerful experimental technique provides an order parameter profile that describes the ordering of lipid acyl chains within the bilayer. A large order parameter means the motion of the acyl chains is strongly constrained, corresponding to tighter molecular packing, whereas small order parameters indicate more disorder and looser packing (8,10–12). For this part of the study, we used deuterium-labeled lipids in PS/PC mixtures identified by x-ray scattering to be in the MLV-ULV transition range. We take advantage of this transition, at which membrane structure is highly sensitive to lipid composition, to identify how Cers modify lipid interactions. By these methods, we determine the effect of two distinct Cer species, C6:0 and C18:1, on the molecular organization and physical properties of PS-containing membranes. To demonstrate the relevance of these findings to efferocytosis, we then use PS/PC model membranes in flow cytometry measurements of phagocytosis by rat AMs. We used both native AMs and AMs pretreated with C6:0 to parallel the cellular biology study in Petrusca et al. (32). The C18:1 Cer was chosen to match the 18:1 chain of lipids used for model vesicles, whereas the short-chain Cer, C6:0, was chosen based on a study reported previously (32), in which it was found that C6:0 in human acellular bronchoalveolar lavage fluid can inhibit AM efferocytosis. By investigating model membranes with various Cer/PS/PC ratios and deuterated species, we show how Cers alter membrane organization and interactions, which could explain, or at least be correlated with, engulfment observations. These studies that integrate experiments with model membranes and cultured cells can lead to a better understanding of the role of membrane interactions in efferocytosis and in phagocytosis in general.

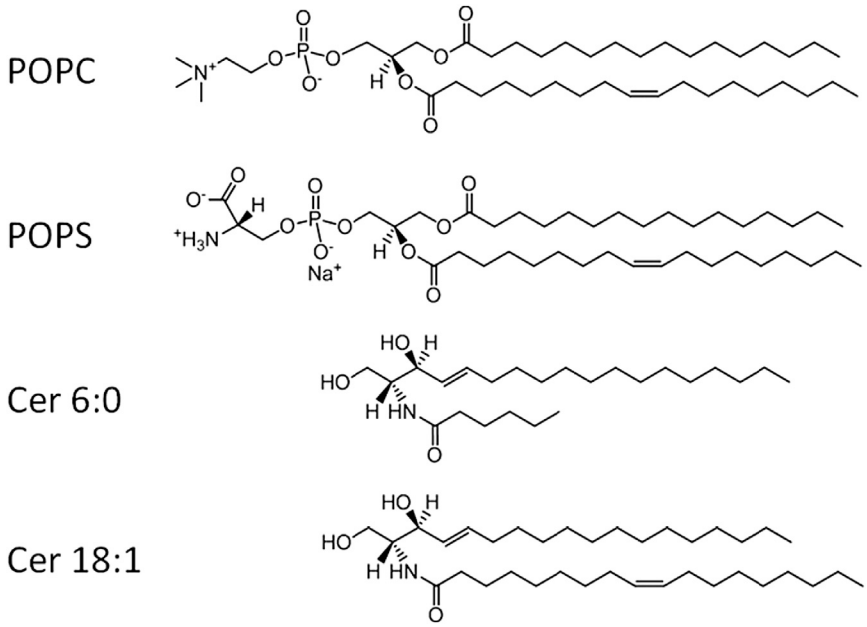

FIGURE 1 Chemical stuctures of model lipid membranes POPC, POPS, Cer6:0, and Cer18:1 used in this study.

MATERIALS AND METHODS

Lipids

1-palmitoyl-2-oleoyl-*sn*-glycero-3-phospho-L-serine (sodium salt) (16:0-18:1PS (POPS) and [$^2H_{31}$]16:0-18:1PS (POPS-d_{31})), 1-palmitoyl-2-oleoyl-*sn*-glycero-3-phosphocholine (16:0-18:1 PC (POPC) and [$^2H_{31}$] 16:0-18:1 PC (POPC-d_{31})), 1,2-dioleoyl-*sn*-glycero-3-phospho-L-serine (sodium salt) (18:1-18:1 PS (DOPS)), 1,2-dioleoyl-*sn*-glycero-3-phosphocholine (18:1-18:1 PC (DOPC)), N-hexanoyl-D-*erythro*-sphingosine (d18:1/6:0 Cer, Cer6:0), N-oleoyl-D-*erythro*-sphingosine (d18:1/18:1(9Z) Cer, Cer 18:1), and 1,2-dioleoyl-*sn*-glycero-3-phosphoethanolamine-N-(7-nitro-2-1,3-benzoxadiazol-4-yl) (ammonium salt) (NBD-DOPE) were purchased from Avanti Polar Lipids (Alabaster, AL). Cambridge Isotope Laboratories (Andover, MA) was the source of deuterium-depleted water.

X-ray scattering

Sample preparation

Lipids were codissolved in chloroform for a total of 20 mg lipid per mixture. Organic solvent was evaporated with argon or nitrogen gas and placed in a vacuum chamber overnight to remove remaining solvent. Resulting lipid films were hydrated in 18.2 MΩ cm deionized H_2O, shelved, and lyophilized. Lipid mixtures (5 mg) were hydrated with 1 mL of 200 mM NaCl (195 mM final concentration) and 25 μL of 200 mM phosphate buffer (4.8 mM final concentration) in 1.5 mL plastic vials with O-ring caps and put through three freeze/thaw cycles. Samples were x-rayed either in plastic tubes or in thin-walled glass capillaries. Samples were allowed to equilibrate for at least 30 min in a home-made temperature-controlled sample holder at 30°C.

Measurements

SAXS measurements were performed using a Bruker Nanostar U instrument with a 1.54 Å Cu source. The x-ray beam was focused by Göbel mirrors and defined by three pinholes, of which the smallest was 750 μm in diameter. Samples were mounted in a home-built temperature-controlled sample holder of accuracy 0.1°C, and data were collected on a HI-STAR wire detector. Scanning times varied from 5 min to 3 h, depending on scattering intensity. SAXS software (Bruker) was used to log the data from the detector. The program FIT2D was used to integrate over the χ angle.

^{2}H NMR spectroscopy

Sample preparation

Lipid mixtures were dissolved in chloroform. They comprised POPC, Cer/POPC (1:10), POPS, Cer/POPS (1:10), POPS/POPC (1:20), and Cer/POPS/POPC (1:1:20) in a mixture of 100 mg total lipid. Each sample included 5 mol % POPC-d_{31} or POPS-d_{31}. Organic solvent was evaporated using argon or nitrogen gas and samples were placed in a vacuum chamber overnight to remove remaining solvent. The dried lipid was hydrated in 100 μL buffer (200 mM NaCl/5 mM phosphate) and deuterium-depleted water (~2 mL) was added to enable measurement of pH, which was adjusted to 7.5 with NaOH. Three lyophilizations in the presence of excess deuterium-depleted water were then performed to remove naturally abundant ^{2}HHO. After finally hydrating to 50 wt %, the resultant samples were transferred to a 5 mm NMR tube that was sealed with a Teflon-coated plug. Samples were allowed to equilibrate for 30 min in a temperature controlled probe at 30°C.

Measurements

Solid-state ^{2}H NMR experiments were performed on a home-built spectrometer (54) operating at 46.0 MHz with a 7 T Oxford Instruments superconducting magnet (Osney Mead, United Kingdom). Spectra were collected with a phase-alternated quadrupolar echo sequence ($90°_x$-τ-$90°_y$-acquire-delay)$_n$ that eliminates spectral distortion due to receiver recovery time (55). Spectral parameters were 90° pulse width, 3.2 μs; separation between pulses, $\tau = 50$ μs; delay between pulse sequences, 1.5 s; sweep width, ± 100 kHz; dataset, 2 K; and number of transients, 40,960.

Analysis of ^{2}H NMR spectra

First moments, M_1 (56), were calculated from powder-pattern spectra with

$$M_1 = \frac{\int_{-\infty}^{\infty} |\omega| f(\omega) d\omega}{\int_{-\infty}^{\infty} f(\omega) d\omega}. \quad (1)$$

Here, $f(\omega)$ represents the line shape as a function of frequency, ω, relative to the central Larmor frequency, ω_0, and in practice, the integration was a summation over the digitized data. The value of M_1 equates, via the static quadrupolar coupling constant, $e^2qQ/h = 167$ kHz, to an average order parameter, $\overline{S}_{CD}$, for the perdeuterated palmitoyl *sn*-1 chain of POPC-d_{31} and POPS-d_{31} in the various mixed membranes according to

$$M_1 = \frac{\pi}{\sqrt{3}}\left(\frac{e^2qQ}{h}\right)\left|\overline{S}_{CD}\right|. \quad (2)$$

To map the variation of order along the chain within the liquid crystalline bilayer, the FFT depaking algorithm was applied to deconvolute the powder pattern signal to an aligned spectrum representative of a planar bilayer (57). The depaked spectrum consists of doublets with quadrupole splittings, $\Delta\nu(\theta)$, that relate to an order parameter, S_{CD}, by

$$\Delta\nu(\theta) = \frac{3}{2}\left(\frac{e^2qQ}{h}\right)|S_{CD}|P_2(\cos\theta), \quad (3)$$

where $\theta = 0^\circ$ specifies the orientation of the bilayer normal relative to the magnetic field and $P_2(\cos\theta)$ is the second-order Legendre polynomial. A smoothed profile of order parameter was then constructed on the basis of integrated intensity assuming order decreases monotonically from the membrane surface toward the terminal methyl in the middle of the membrane (58).

Flow cytometry

Sample preparation

Model membranes were prepared in the same manner as the x-ray samples, except that they were hydrated with Ham's F12K medium and a fluorescent tag (1.1 μM NBD-DOPE) was included.

Cell cultures

The rat AM cell line NR8383 (ATCC) was maintained in Ham's F12K medium containing L-glutamine (2 mM), sodium bicarbonate (1.5 g/L), and heat-inactivated fetal bovine serum (15%). Cell counts and viability were determined using Trypan blue dye exclusion, and cell counting was performed using a hemocytometer. All chemical reagents were purchased from Sigma-Aldrich (St. Louis, MO), unless otherwise stated. Macrophages and target model membranes (lipid vesicles) were cocultured for 1 h. After coculturing, nonengulfed liposomes were extensively washed with cold phosphate-buffered saline (PBS), and macrophages were harvested by scraping and fixed with paraformaldehyde (1%). For quenching, we followed the method by Hed et al. (59) that utilizes Trypan blue, which is impermeable to an intact cell membrane, to eliminate the fluorescence of adherent liposomes. Since the concentration of the incorporated NBD-PE lipid is very small, a solution containing 0.04% Trypan blue is sufficient to quench the adherent fluorescent signal, allowing differentiation between apoptotic target attachment/binding and ingestion.

Incubation of cells with Cer

Rat AMs (NR8383) were cultured in six-well dishes with 1 mL of Ham's F-12 medium containing 15% fetal bovine serum (full medium). At the time of the experiment, full medium was removed and Ham's F-12 medium containing 2% fetal bovine serum (low-serum medium) was added and allowed to incubate for 1 h. Then, C6:0 dissolved in ethanol or vehicle control (0.0001% ethanol) was added in appropriate amounts to AMs for a working concentration of 10 μM and allowed to incubate for 4 h. At this time, the medium was removed and new low-serum medium was added along with target model membranes (lipid vesicles) and allowed to incubate with AMs for 1 h.

Flow cytometry measurements

Efferocytosis was quantified with a Cytomics FC500 cytofluorometer (Beckman Coulter, Fullerton, CA) with CXP software, using a previously-described method (60). Engulfment indices were calculated from fluorescence versus forward scatter plots with a gate (threshold) set at the autofluorescence distribution of macrophages alone. Anything above this gate represents a fluorescence signal due to engulfment of lipid vesicles. Autofluorescence gates were set with macrophages alone on a FS/FL1 parameter panel that discriminates the sample by size and fluorescence, respectively (low autofluorescence, large size for macrophages alone). The population of macrophages alone showed sizes much larger than those of liposomes alone. In addition, liposomes alone had a much narrower distribution of sizes, with the lowest fluorescent signal much higher than that of autofluorescent macrophages. The population of macrophages that ingested liposomes was distributed on the FS/FL1 panel above the fluorescence level of macrophages alone (FL1), also showing an elevation in size (FS) when compared to macrophages alone. Results were expressed as percentage of macrophages showing ingested vesicles.

Fluorescence microscopy

Model membrane mixtures that included fluorescent lipid were hydrated with buffer solutions as for x-ray and NMR samples. A drop of 20 μL of the vortexed suspension was placed on a slide and allowed to equilibrate for a short period of time (1–10 min). The slides were then viewed on a Nikon Eclipse 80-i at 10× and 20× magnification. Images of model membranes engulfed by macrophages were obtained by performing the engulfment experiment with macrophages that were plated on coverslips. At the end of coculture, medium was aspirated and PBS containing Trypan blue was added to quench extracellular fluorescence. Next, PBS was aspirated and the coverslips were carefully flipped onto slides over a drop of DAPI Slowfade Gold. Slides were then sealed with nail polish and viewed in the same manner as above, after the nail polish was allowed to dry.

RESULTS

X-ray scattering

SAXS profiles of lipid vesicles with various PS/PC ratios are shown for DOPS/DOPC mixtures in Fig. 2 *A*. At low PS content, scattering profiles present two prominent peaks at scattering angles (2θ) in the range ~1.3–1.4° and ~2.6–2.8°, corresponding to a *D*-spacing of ~63–65 Å. The two equally spaced peaks, called Bragg peaks, are the signature of MLVs with regular spacing between bilayers. This is the case for samples with low PS content, as indicated by the vertical dashed lines in Fig. 2 *A*. These scattering (Bragg) peaks appear at angles satisfying Bragg's law,

$$2D\sin\theta = h\lambda, \quad (4)$$

where D is the lamellar repeat distance, θ is the incident angle of the x-ray beam, λ is the x-ray wavelength, and h is an integer index. For MLVs in the fluid state, the two scattering peaks observed correspond to $h = 1$ and $h = 2$. Higher-order peaks are absent due to membrane undulation (14,18). Because of scattering geometry, x-ray profiles are conventionally plotted versus twice the scattering angle (2θ). The results in Fig. 2 *A* show that as the PS content in mixed membranes increases, scattering

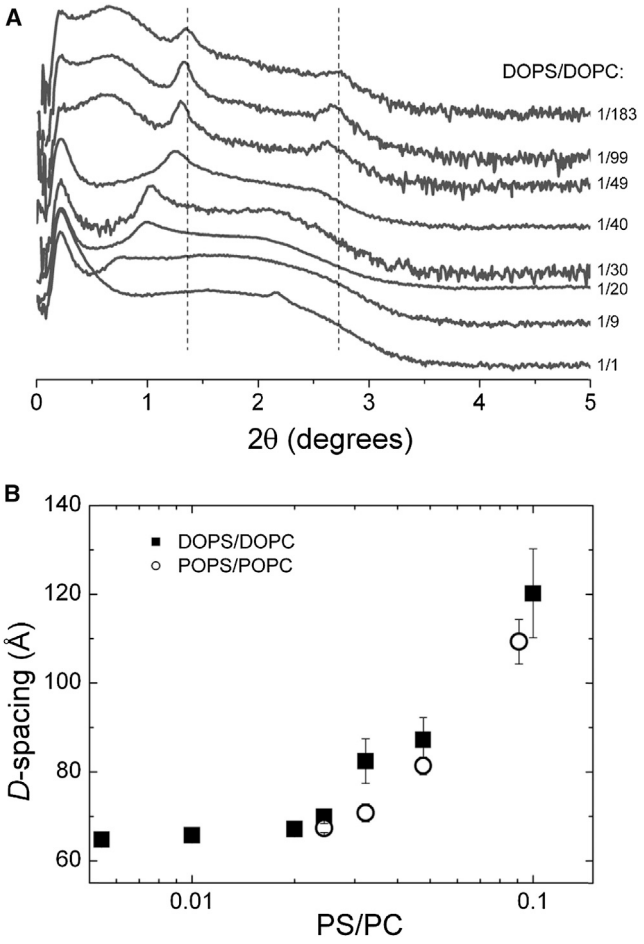

FIGURE 2 (*A*) SAXS of DOPS/DOPC mixtures at 30°C in 200 mM NaCl solutions. Scattering intensity is plotted versus scattering angle 2θ and is presented in arbitrary units with curves offset vertically for clarity. Vertical dashed lines indicate the position of scattering peaks for the uppermost curve. (*B*) Plot of lamellar repeat spacings versus PS/PC molar ratio in DOPS/DOPC (*squares*) and POPS/POPC mixtures (*circles*).

peaks shift to smaller 2θ values (smaller angles). Since the scattering angle and the repeat spacing are inversely proportional (according to Eq. 4), it means that the equilibrium distance between membranes increases with PS content (Fig. 2 *B*). This behavior is expected because of the electrostatic repulsion generated by the charged PS lipids (10), and it is seen with both DOPS/DOPC and POPS/POPC mixtures. The MLVs are said to swell with the addition of PS. The disappearance of Bragg peaks indicates catastrophic swelling (unbinding), where MLVs break up into ULVs and possibly other disordered structures (25,61–63). The exact transition point from MLVs to ULVs is generally difficult to identify, but the scattering profiles in Fig. 2 indicate that it occurs for PS/PC molar ratios between 1:20 and 1:10. We also note that at high PS content, x-ray scans present some additional features, such as the small peak at $2\theta \sim 2.2°$, which cannot be indexed. These could correspond to a small fraction of less defined structures (possibly nonlamellar), as discussed in Steiner et al. (25).

MLV and ULV structures can also be distinguished by optical microscopy of fluorescently labeled vesicles, in accord with results from x-ray scattering (Fig. 3). Although these images cannot reveal the inner structure of lipid vesicles, it is clear that POPC alone forms aggregates at least 10 times larger than those formed by POPS.

A direct way to determine whether Cer affects membrane interactions is to incorporate it into PS/PC mixtures in the MLV-ULV transition range and measure changes in x-ray scattering peaks. For these measurements, we have chosen POPS/POPC mixtures that behave similarly to DOPS/DOPC (Fig. 2 *B*), because they are also suitable for ^{2}H NMR measurements (see below). X-ray measurements of

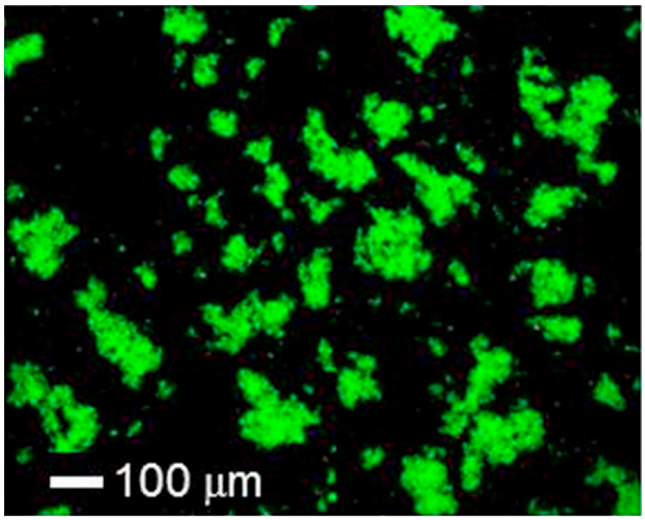

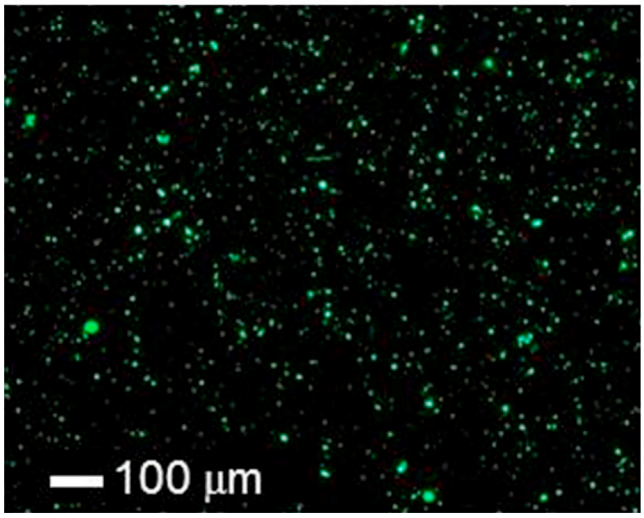

FIGURE 3 Optical microscopy images of fluorescently labeled POPC MLVs (*upper*) and POPS ULVs (*lower*) in 200 mM NaCl, pH 7.5, at room temperature.

Cer/POPS/POPC mixtures are shown in Fig. 4 for PS/PC molar ratios of 1:20 (Fig. 4 *A*) and 1:10 (Fig. 4 *B*). For both mixtures, addition of Cer to a 1:1 Cer/PS ratio shifts the positions of Bragg peaks to larger values of the scattering angle corresponding to reduced interlamellar distances (Eq. 4). In the case of 1:10 PS/PC mixtures (Fig. 4 *B*), addition of Cer6:0 generates sharper Bragg peaks than addition of Cer18:1, indicating that Cer6:0 is a stronger stabilizer of MLVs than Cer18:1. A similar situation occurs for 1:20 PS/PC mixtures (Fig. 4 *A*), although the differential in effects is diminished, since the 1:20 PS/PC mixture is predominantly composed of MLVs.

The observed effect of Cer on the stability of MLVs can be due to alteration of any of the intermembrane forces mentioned in the Introduction, namely van der Waals attraction, electrostatic repulsion, and entropic terms (hydration and undulation) (10,14). However, regardless of the exact mechanism, x-ray data show that Cers modify the balance of attractive and repulsive forces between neighboring membranes by stabilizing MLV structures in the MLV-ULV transition range, corresponding to PS/PC ratios between 1:20 and 1:10. We will now focus on these lipid mixtures for a thorough characterization of lipid packing by solid-state ^{2}H NMR.

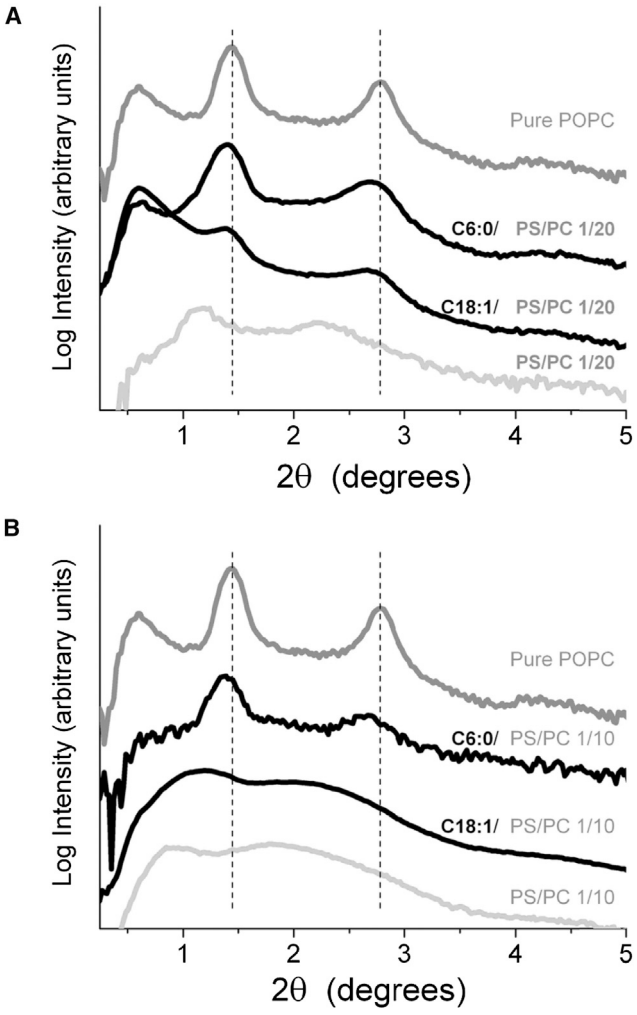

FIGURE 4 X-ray scattering of Cer/POPS/POPC mixtures at 30°C. Scattering curves have been shifted vertically for clarity. The uppermost curve shows pure POPC and the lower curves show PS/PC mixtures with molar ratios 1:20 (*A*) and 1:10 (*B*).

^{2}H NMR

Molecular organization within membranes was examined in detail by solid-state ^{2}H NMR spectroscopy. Our probe was either POPC-d_{31} or POPS-d_{31} (analogs of the respective phospholipids with a perdeuterated palmitic acid *sn*-1 chain) and comprised 5 mol % of the total lipid. The samples were aqueous dispersions containing 50% lipid by weight.

^{2}H NMR spectra were recorded for POPC-d_{31} in POPC, Cer6:0/POPC (1:10 mol), and Cer18:1/POPC (1:10 mol), for POPS-d_{31} in POPS, Cer6:0/POPS (1:10 mol), and Cer18:1/POPS (1:10 mol), and for POPC-d_{31} and POPS-d_{31} in POPS/POPC (1:20 mol), Cer6:0/POPS/POPC (1:1:20 mol), and Cer18:1/POPS/POPC (1:1:10 mol), at 30°C. All recorded spectra have a similar shape that is a signature for the saturated *sn*-1 chain of phospholipids in the lamellar liquid crystalline phase (56). Fig. 5 shows representative examples in which the signal is the function $f(\omega)$ described in Materials and Methods, plotted as a function of frequency, ω, relative to the central Larmor frequency, ω_0, that characterizes the interaction of the deuterium nucleus with the magnetic field. The different peaks and shoulders in the line shape correspond to various carbon-deuterium bonds along the labeled acyl chain. There are well-defined edges at $\pm$15–20 kHz that correspond to a plateau region of slowly decreasing order in the upper portion (C2–10) of the chain, whereas the pairs of peaks within the spectrum reflect progressively more disorder toward the bottom of the chain in the lower portion (C11–16). From depaked spectra (64), we calculate order parameter values for individual carbon segments as shown in the order parameter profiles in Fig. 6 and explained below. Order parameters are between 0.2 and 0.25 for carbon segments next to lipid headgroups (in the plateau region) and decrease to significantly smaller values toward the methyl group at the bilayer center.

POPC and POPS

Experiments were performed on POPC and POPS individually to provide a baseline for interpretation of the behavior seen with each phospholipid in mixed membranes. The spectra for POPC-d_{31} in POPC (Fig. 5 *A*) and POPS-d_{31} in POPS (Fig. 5 *B*) illustrate in each case the characteristic form. The spectrum for POPS is wider, indicative of greater order within the bilayer. This assessment is corroborated by the average order parameters ($\overline{S}_{CD} = 0.172$ for POPS-d_{31} and $\overline{S}_{CD} = 0.136$ for POPC-d_{31}) calculated from the first moments (see Table 1) and agrees with earlier reports on

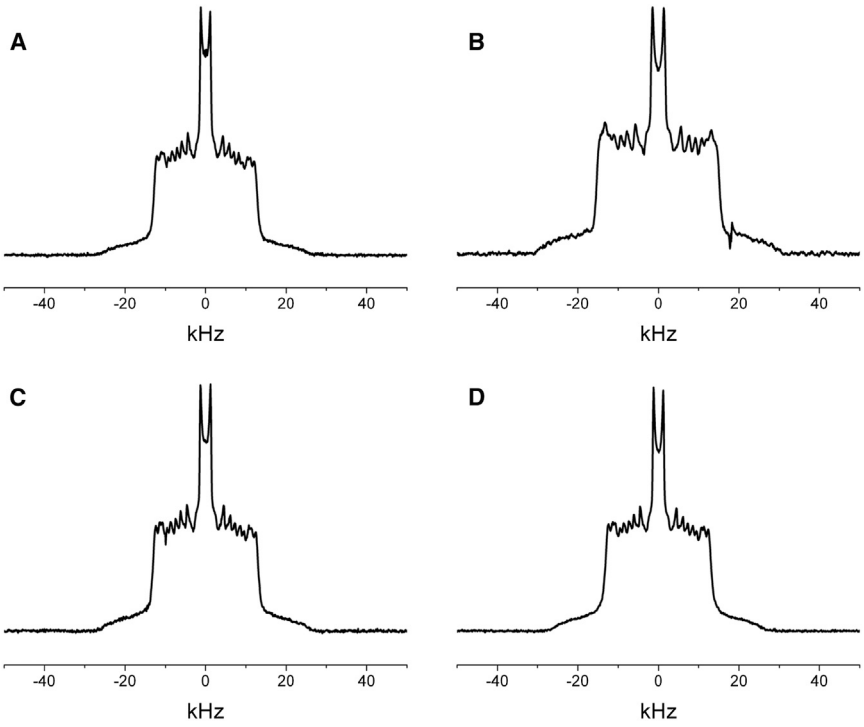

FIGURE 5 ^{2}H NMR spectra of 50 wt % aqueous dispersions of POPC-d_{31} in POPC (*A*), POPS-d_{31} in POPS (*B*), POPC-d_{31} in POPS/POPC (1:20) (*C*), and POPS-d_{31} in POPS/POPC (1:20) (*D*). Samples were prepared in phosphate buffer at pH 7.5 and spectra were acquired at 30°C.

POPS and POPC lipids (65), as well as with measurements on SOPS and SOPC (10).

A general elevation in order throughout the POPS bilayer is responsible for the larger average order parameter, as can be seen from the smoothed order parameter profiles determined for POPC-d_{31} (Fig. 6 *A*) in POPC and for POPS-d_{31} in POPS (Fig. 6 *B*). Both profiles are typical of phospholipid bilayers in the lamellar liquid crystalline state (66), displaying a plateau region of approximately constant order in the upper portion of the chain (C2–10) followed by more steeply decreasing order in the lower portion (C11–16).

The spectra obtained for POPC-d_{31} in Cer6:0/POPC and Cer18:1/POPC (1:10 mol) and for POPS-d_{31} in

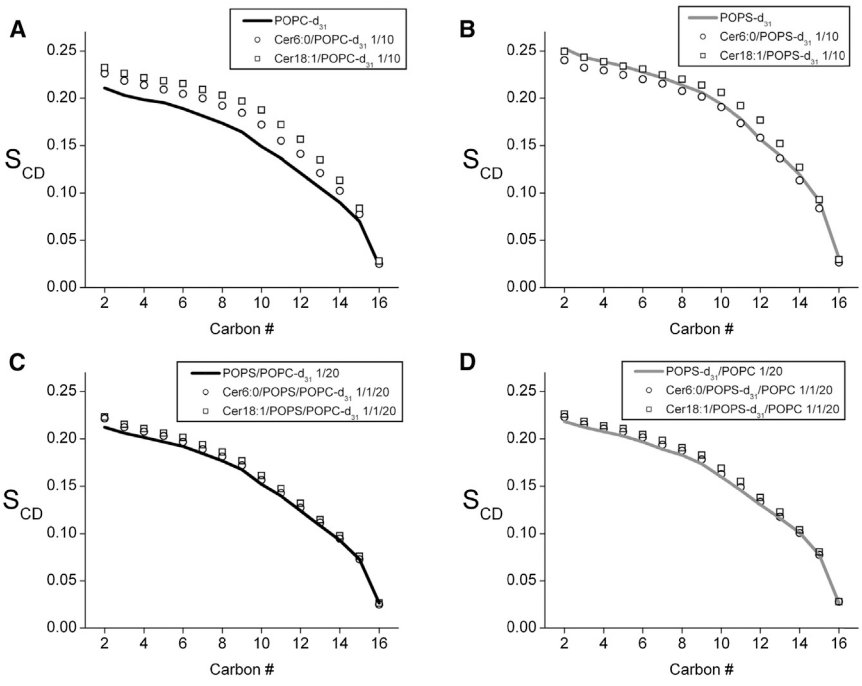

FIGURE 6 Smoothed profile of order parameter S_{CD} versus position along the *sn*-1 chain at 30°C for (*A*) POPC-d_{31} in POPC (*solid line*), Cer6:0/POPC (1:10) (*open circles*), and Cer18:1/POPC (1:10) (*open squares*); (*B*) POPS-d_{31} in POPS (*solid line*), Cer6:0/POPS (1:10) (*open circles*), and Cer18:1/POPS (1:10) (*open squares*); (*C*) POPC-d_{31} in POPS/POPC (1:20) (*solid line*), Cer6:0/POPS/POPC (1:1:20) (*open circles*), and Cer18:1/POPS/POPC (1:1:20) (*open squares*); and (*D*) POPS-d_{31} in POPS/POPC (1:20) (*solid line*), Cer6:0/POPS/POPC (1:1:20) (*open circles*), and Cer18:1/POPS/POPC (1:1:20 mol) (*open squares*).

TABLE 1 Average order parameters, $\overline{S}_{CD}$, derived from ^{2}H NMR spectra

	$\overline{S}_{CD}$		
Membrane	No Cer	Cer 6:0 (1:10)	Cer 18:1 (1:10)
POPC-d_{31}	0.136	0.150	0.162
POPS-d_{31}	0.172	0.163	0.174
	No Cer (1:20)	Cer 6:0 (1:1:20)	Cer 18:1 (1:1:20)
POPS/POPC-d_{31}	0.143	0.142	0.148
POPS-d_{31}/POPC	0.146	0.146	0.149

Order parameters are presented for POPC-d_{31} in POPC and POPS-d_{31} in POPS in the absence of ceramide and in the presence of Cer 6:0 and Cer 18:1 (1:10), and for POPC-d_{31} and POPS-d_{31} in mixed POPS/POPC (1:20) vesicles in the absence of ceramide and in the presence of Cer 6:0 and Cer 18:1 (1:1:20 mol) at 30°C.

Cer6:0/POPS and Cer18:1/POPS (1:10 mol) resemble those collected in the absence of Cer (data not shown), implying that there is no change in the general form of the order parameter profile. This assessment is confirmed by the order parameter profiles plotted in Fig. 6. The profiles do reveal that POPC and POPS respond differently to the addition of Cer. Acyl chain motion in POPC is restricted by Cer6:0 and, to a greater extent, Cer18:1 (Fig. 6 *A*). The corresponding values for the average order parameter are $\overline{S}_{CD} = 0.150$ with Cer 6:0, an increase of 10%, and $\overline{S}_{CD} = 0.162$ with Cer18:1, an increase of 19% (Table 1). This behavior is consistent with membrane ordering due to N-palmitoyl-sphingosine (Cer16:0) seen in a previous study with POPC-d_{31} (49). In contrast, Cer6:0 disorders POPS, whereas Cer18:1 slightly orders it (Fig. 6 *B*). The average order parameter is $\overline{S}_{CD} = 0.163$ in the presence of Cer6:0 and $\overline{S}_{CD} = 0.174$ in the presence of Cer18:1, representing a decrease of 5% with Cer6:0 and an increase of 1% with Cer18:1 (Table 1). To the best of our knowledge, the effect of Cer on molecular organization in PS bilayers has not been described before.

POPS/POPC mixtures

The spectra for POPC-d_{31} (Fig. 5 *C*) and POPS-d_{31} (Fig. 5 *D*) in POPS/POPC (1:20 mol) have the same overall shape observed with pure phospholipids. There is a slight increase in order for POPC-d_{31} ($\overline{S}_{CD} = 0.143$) and a substantial reduction in order for POPS-d_{31} ($\overline{S}_{CD} = 0.146$) in the mixed membrane relative to the pure systems, resulting in average order parameters that are very similar (Table 1) and an order parameter profile for POPS-d_{31} (Fig. 6 *D*) that lies just above and almost overlaps that of POPC-d_{31} (Fig. 6 *C*) in the mixture. No variation due to the introduction of Cer is seen in the general form of the spectra for POPC-d_{31} and POPS-d_{31} in Cer6:0/POPS/POPC (1:1:20 mol) and Cer18:1/POPS/POPC (1:1:20 mol) (data not shown). The average order parameters calculated (Table 1) demonstrate that the effect of Cer on the order of either phospholipid in the mixed system is minimal. The value of $\overline{S}_{CD}$ for POPC-d_{31} and POPS-d_{31} is essentially unaltered after the addition of Cer6:0 ($\overline{S}_{CD} = 0.142$ and 0.146, respectively), whereas Cer18:1 causes only a small increase (<~3%) ($\overline{S}_{CD} = 0.148$ and 0.149, respectively). These changes, albeit minor, are spread throughout the perdeuterated palmitic *sn*-1 chain, as depicted in the order parameter profiles in Fig. 6.

Flow cytometry

Engulfment of fluorescently labeled POPS/POPC model membranes by rat AMs (cell line NR8383) was investigated by coincubation followed by flow cytometry. Coculturing of macrophages and target lipid vesicles was limited to 1 h to minimize intracellular digestion. An example of engulfment visualized by fluorescence microscopy is shown in Fig. 7. Fluorescently labeled POPS/POPC lipid vesicles are seen to incorporate well within rat AMs, as determined by 3D inspection of images.

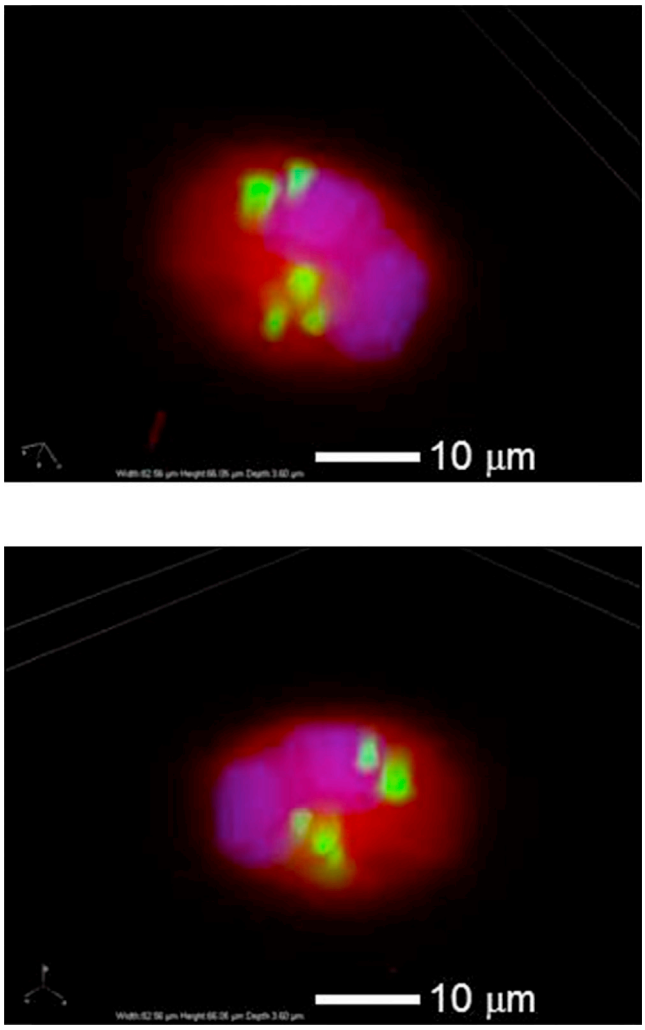

FIGURE 7 Two different fluorescence microscope images of a single rat AM cell (*red*, cytoplasm autofluorescence; blue, nucleus) engulfing several fluorescently labeled POPS/POPC lipid vesicles (*green*).

Engulfment indices (see Materials and Methods) are shown in Fig. 8 as a function of the PS/PC ratio in model vesicles. The engulfment index represents the percentage of macrophages that showed ingestion of fluorescent labels. Washing after incubation eliminated free lipid vesicles ensuring that only engulfed labels were detected during flow cytometry measurements. As shown in Fig. 8 *A*, the engulfment increases sharply with PS content, from <10% in the absence of PS to 50% in the 1:1 PS/PC mixture and to >90% in PS alone, consistent with the expectation that macrophages are able to recognize PS lipids. These results, however, are also influenced by the geometry of lipid vesicles. As seen by x-ray scattering (Fig. 2), PS/PC vesicles are primarily in MLV form at small PS content and in ULV form at high PS content. It is possible that engulfment is reduced in the case of large MLVs.

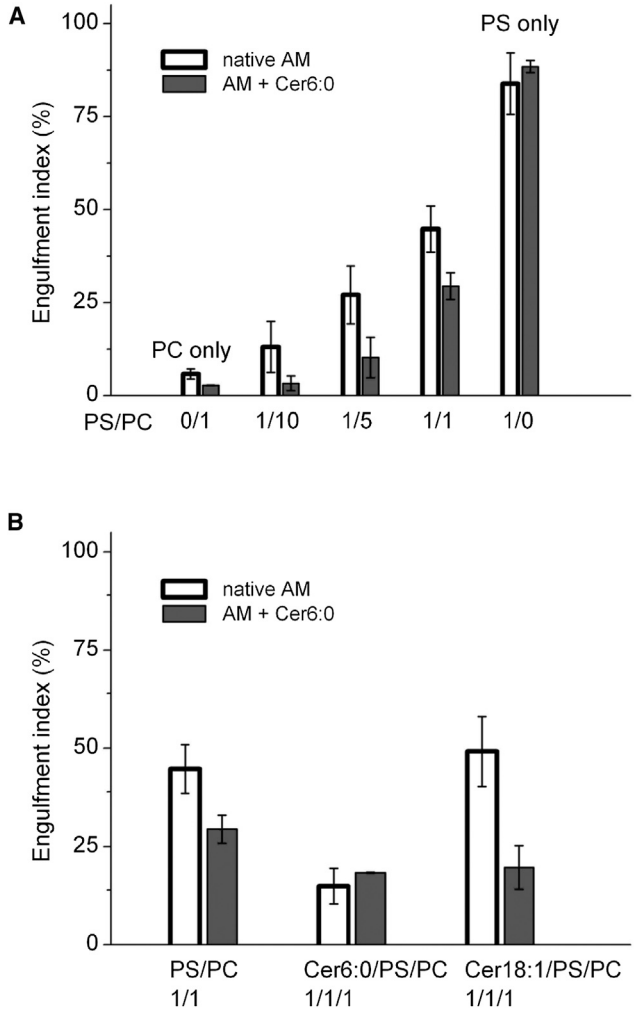

FIGURE 8 (*A*) Engulfment of POPS/POPC vesicles by macrophages as a function of PS/PC ratio. (*B*) Engulfment of 1:1 POPS/POPC vesicles as a function of added Cer to target vesicles as indicated on the horizontal axis. Open bars represent measurements with native macrophages and solid bars measurements with macrophages pretreated with Cer6:0.

Fig. 8 *A* also shows that the engulfment index decreases noticeably when macrophages are preincubated with C6:0 (see Materials and Methods), consistent with the reported inhibitory effect of macrophage exposure to various Cer species on efferocytosis (32). The largest effect due to preincubation is measured for PS/PC ratios around 1:10, in the range where x-ray measurements showed a transition from MLVs to ULVs. This result indicates that in addition to specific PS recognition by macrophages, the size of the lipid vesicles also affects engulfment.

Finally, Fig. 8 *B* shows engulfment results for 1:1 PS/PC mixtures containing C6:0 or C18:1 at a ratio of Cer to PS of 1:1. Results are compared for normal macrophages and macrophages pretreated with C6:0. There is a noticeable reduction of engulfment with addition of C6:0, either to vesicles alone or to both vesicles andmacrophages. Addition of C18:1 to vesicles reduces engulfment for macrophages treated with C6:0 but not for normal macrophages.

DISCUSSION

Engulfment measurements show that the presence of PS lipids in model membranes is indeed favorable for uptake of vesicles by macrophages (Fig. 8 *A*). In contrast, addition of Cer 6:0 to either lipid vesicles or AMs reduces model vesicle engulfment similar to the case for apoptotic body engulfment (32). We note, however, that pretreatment of macrophages with Cer and incorporation of Cer into model vesicles can have different modes of action. Furthermore, the situation can be complicated by the possibility of Cer exchange between macrophages and model vesicles. The observed engulfment reduction in the presence of Cer is correlated to modification of lipid interactions, as shown by x-ray and NMR: net membrane repulsion decreases and lipid ordering within membranes increases slightly. Addition of Cer to lipid bilayers can affect interactions between membrane surfaces as well as lipid-lipid interactions within membranes. However, since intramembrane forces (probed by NMR) are much stronger than intermembrane forces (probed by x-ray) (10,67), they are less sensitive to perturbations such as addition of Cer.

The observation that fully functional macrophages engulf model lipid vesicles that lack proteins with a specificity similar to that for apoptotic cells demonstrates the importance of lipid interactions in efferocytosis. The process of engulfment by macrophages relies on favorable interactions between lipid membranes, and this process must overcome two important factors: 1), the intrinsic repulsion between hydrated membrane surfaces (63); and 2), elastic deformations at the local or global level, possibly accompanied by adjustment of local lipid composition and formation of lipid domains. A precise quantification of membrane mechanics is generally a difficult task even in simple lipid bilayers (see, e.g., literature on membrane fusion barrier (68).).

Here, we took to our knowledge the first steps in identifying relevant features of macrophage engulfment of model lipid vesicles made of PC, PS, and Cer. Using SAXS, we determined that membrane interactions are affected by PS and Cer content (Figs. 2 and 4). Using solid-state ^{2}H NMR, we measured how acyl chain ordering differs in PS/PC mixtures compared to pure PC and PS lipid bilayers, and showed to what extent ordering is modified by Cer (Fig. 6). Finally, we showed by flow cytometry that macrophages can recognize and engulf model lipid vesicles and that engulfment is affected by PS content and by the presence of Cer either in vesicles or in macrophages themselves (Fig. 8).

Lipid vesicles in this study lack the complexity of real biological cells. This fact has both advantages and disadvantages. The advantage is that molecular composition is known and can be varied systematically. The disadvantage is that important factors are left out. For example, the presence on the outer cell membranes of proteins and glycosyl structures that are certainly relevant to the engulfment process is ignored in the model membranes. In addition, interaction with serum proteins used in the engulfment assay may have important effects. However, these factors cannot be addressed all at once but will require systematic increases in the complexity of the model system in future studies. Still, at any level of complexity (or lack thereof) a comparison between PS and PC lipids is still warranted given that all other parameters are kept the same.

Our data show that although engulfment by macrophages is most effective in the case of specific interactions (such as interactions with PS lipids), nonspecific interactions with generic PC lipid membranes can also lead to marginal levels of engulfment (Fig. 8). In physiological conditions, healthy macrophages are proficient in engulfing apoptotic bodies via efferocytosis despite the fact that apoptotic cells (e.g., leukocytes or endothelial cells) might contain higher levels of Cers than nondying cells (69,70). However, the type of Cer species in the target to be engulfed may determine the efficacy of engulfment, as shown in Fig. 8, where addition of C6:0 to model membranes caused a dramatic and reproducible decrease of engulfment, whereas addition of C18:1 did not. It is possible that this differential effect of Cers is due to the greater chain mismatch between Cer and POPS/POPC lipids in the case of C6:0.

In pathological conditions associated with macrophage dysfunction, such as upon exposure of lungs to cigarette smoke, the Cer content of the macrophage itself is increased (upregulated), with negative consequences: whereas AMs do not die when Cer is increased, their efferocytosis function is impaired by alteration of the process of recruitment of cytoskeletal proteins at the plasma membrane (32). The fact that Cer induces impairment of macrophage efferocytosis of model lipid vesicles suggests Cer may not alter recognition of specific protein ligands on apoptotic targets by receptors on the macrophages, but that by interacting with PS lipids, Cer may have effects on membrane interactions as a whole, as indicated by x-ray scattering measurements (Fig. 2). In this respect, the main purpose of the x-ray experiments was to identify a range of PS/PC ratios near the transition from MLVs to ULVs, where a significant change in vesicle shape and size occurs, because it is in this range of concentrations that PS/PC membranes are expected to be most sensitive to perturbations created by addition of Cer.

As shown in Fig. 8, the engulfment index increases with PS content as expected based on the ability of macrophages to recognize PS lipids. However, in addition to specific recognition between lipids and macrophages, the larger engulfment index in the presence of PS can also be explained by the fact that increased PS content destabilizes MLVs in favor of ULVs, making them more susceptible to fusion with macrophages. At this length scale, however, x-ray scattering is unable to distinguish between homogeneous and heterogeneous (domain-forming) lipid mixtures. We therefore turned to solid-sate NMR spectroscopy for a thorough analysis of lipid packing. We found that addition of either PS or, to a smaller degree, Cer to PC membranes increases acyl chain order. Increased acyl chain order leads to thicker bilayers and generally to increased membrane rigidity (10) possibly affecting membrane fusion during engulfment.

The NMR results for the PS/PC mixtures can be discussed in terms of lipid domains. First, we note that only a single spectral component is observed for either POPC-d_{31} or POPS-d_{31} in PS/PC mixtures. This can be explained by formation of POPS-rich/POPC-poor nanoscale domains within a POPC-rich/POPS-poor host membrane. Fast exchange mediated by lateral diffusion of POPC-d_{31} or POPS-d_{31} between the membrane environments would produce a spectrum that is a population-weighted average (54). Preferential incorporation into POPS-rich domains would then explain the lack of response to the introduction of Cer, particularly Cer18:1, observed for POPC-d_{31} in the mixed system compared to the pure one. In essence, Cer is being hidden from POPC. We admit that our interpretation is not definitive. Other explanations exist in principle. We rule out the possibility that POPC and POPS are totally demixed, because the average order parameter measured for POPC-d_{31} and POPS-d_{31} in the mixture differs from the corresponding values measured in the pure membranes (Table 1). Completely homogenous mixing, at the opposite extreme, cannot be discounted, since the small differential in order measured between POPC-d_{31} and POPS-d_{31} in the same mixed system may reflect an intrinsic disparity in molecular conformation associated with a PC versus a PS headgroup. However, based on the substantial increase in average order parameter seen for POPC-d_{31} upon adding Cer to POPC alone, we argue that Cer would be expected to have a larger effect upon POPC-d_{31} in POPC/POPS if the membrane were homogeneously mixed.

We should also note that the water content in the NMR samples was restricted to 50% to enhance the NMR signal. Although this water content is sufficient to fully hydrate PC membranes, it corresponds to less than full hydration for membranes containing PS lipids. To properly quantify lipid interactions, more systematic measurements are needed to map the phase diagram of Cer/PS/PC mixtures. Ternary lipid phase diagram are notoriously difficult to map and require extensive measurements (71). However, based on the selection of lipid mixtures presented in this work, we conclude that the role of PS and of Cer in phagocytosis is based on modification of membrane physical properties, including interactions at large length scales as well as local lipid ordering and possible domain formation. These results indicate that controlling Cer levels or species content may lead to more efficient efferocytosis and thereby attenuate tissue inflammation in conditions of increased apoptosis and impaired macrophage function, such as lung emphysema. Having established the feasibility of using model membranes as apoptotic targets for AMs, this methodology can be used in future studies to investigate more complex lipid mixtures including, for example, sphingomyelin and cholesterol.

We acknowledge Bruce D. Ray and Smita Soni for their help and advice.

Funding for this work was contributed by the Indiana University Purdue University Indianapolis Membrane Biosciences Signature Center (H.I.P., I.P., and S.R.W.), the American Heart Association (grant 0826103G to D.P.), and the National Institutes of Health (grants RO1HL077328 to I.P., and R21 DA029249 to I.P. and H.I.P.).

REFERENCES

1. Aderem, A., and D. M. Underhill. 1999. Mechanisms of phagocytosis in macrophages. *Annu. Rev. Immunol.* 17:593–623.
2. Flannagan, R. S., V. Jaumouille, and S. Grinstein. 2012. The cell biology of phagocytosis. *Annu. Rev. Pathol.* 7:61–98.
3. Lam, J., M. Herant, …, V. Heinrich. 2009. Baseline mechanical characterization of J774 macrophages. *Biophys. J.* 96:248–254.
4. Fadok, V. A., A. de Cathelineau, …, D. L. Bratton. 2001. Loss of phospholipid asymmetry and surface exposure of phosphatidylserine is required for phagocytosis of apoptotic cells by macrophages and fibroblasts. *J. Biol. Chem.* 276:1071–1077.
5. Fadok, V. A., D. R. Voelker, …, P. M. Henson. 1992. Exposure of phosphatidylserine on the surface of apoptotic lymphocytes triggers specific recognition and removal by macrophages. *J. Immunol.* 148:2207–2216.
6. Henson, P. M., D. L. Bratton, and V. A. Fadok. 2001. The phosphatidylserine receptor: a crucial molecular switch? *Nat. Rev. Mol. Cell Biol.* 2:627–633.
7. Petrache, H. I. 2012. Lipid bilayer structure. *In* Comprehensive Biophysics, Volume 5. Membranes. L. Tamm, editor. Elsevier, pp. 3–15.
8. Petrache, H. I., A. Salmon, and M. F. Brown. 2001. Structural properties of docosahexaenoyl phospholipid bilayers investigated by solid-state ^{2}H NMR spectroscopy. *J. Am. Chem. Soc.* 123:12611–12622.
9. Nagle, J. F., and S. Tristram-Nagle. 2000. Structure of lipid bilayers. *Biochim. Biophys. Acta.* 1469:159–195.
10. Petrache, H. I., S. Tristram-Nagle, …, J. F. Nagle. 2004. Structure and fluctuations of charged phosphatidylserine bilayers in the absence of salt. *Biophys. J.* 86:1574–1586.
11. McCabe, M. A., G. L. Griffith, …, S. R. Wassall. 1994. ^{2}H NMR studies of isomeric ω3 and ω6 polyunsaturated phospholipid membranes. *Biochemistry.* 33:7203–7210.
12. Petrache, H. I., S. W. Dodd, and M. F. Brown. 2000. Area per lipid and acyl length distributions in fluid phosphatidylcholines determined by ^{2}H NMR spectroscopy. *Biophys. J.* 79:3172–3192.
13. Rajamoorthi, K., H. I. Petrache, …, M. F. Brown. 2005. Packing and viscoelasticity of polyunsaturated ω-3 and ω-6 lipid bilayers as seen by ^{2}H NMR and x-ray diffraction. *J. Am. Chem. Soc.* 127:1576–1588.
14. Petrache, H. I., N. Gouliaev, …, J. F. Nagle. 1998. Interbilayer interactions from high-resolution x-ray scattering. *Phys. Rev. E Stat. Phys. Plasmas Fluids Relat. Interdiscip. Topics.* 57:7014–7024.
15. Petrache, H. I., T. Zemb, …, V. A. Parsegian. 2006. Salt screening and specific ion adsorption determine neutral-lipid membrane interactions. *Proc. Natl. Acad. Sci. USA.* 103:7982–7987.
16. LeNeveu, D. M., R. P. Rand, and V. A. Parsegian. 1976. Measurement of forces between lecithin bilayers. *Nature.* 259:601–603.
17. Cowley, A. C., N. L. Fuller, …, V. A. Parsegian. 1978. Measurement of repulsive forces between charged phospholipid bilayers. *Biochemistry.* 17:3163–3168.
18. Petrache, H. I., S. Tristram-Nagle, …, V. A. Parsegian. 2006. Swelling of phospholipids by monovalent salt. *J. Lipid Res.* 47:302–309.
19. Lis, L. J., M. McAlister, …, V. A. Parsegian. 1982. Interactions between neutral phospholipid bilayer membranes. *Biophys. J.* 37: 657–665.
20. Rand, R. P., and V. A. Parsegian. 1989. Hydration forces between phospholipid bilayers. *Biochim. Biophys. Acta.* 988:351–376.
21. Parsegian, V. A. 2006. Van Der Waals Forces: A Handbook for Biologists, Chemists, Engineers, and Physicists. Cambridge University Press, New York.
22. Browning, J. L., and J. Seelig. 1980. Bilayers of phosphatidylserine: a deuterium and phosphorus nuclear magnetic resonance study. *Biochemistry.* 19:1262–1270.
23. MacDonald, R. C., S. A. Simon, and E. Baer. 1976. Ionic influences on the phase transition of dipalmitoylphosphatidylserine. *Biochemistry.* 15:885–891.
24. Hope, M. J., and P. R. Cullis. 1980. Effects of divalent cations and pH on phosphatidylserine model membranes: a ^{31}P NMR study. *Biochem. Biophys. Res. Commun.* 92:846–852.
25. Steiner, A., P. Szekely, …, U. Raviv. 2012. Entropic attraction condenses like-charged interfaces composed of self-assembled molecules. *Langmuir.* 28:2604–2613.
26. Koerner, M. M., L. A. Palacio, …, H. I. Petrache. 2011. Electrodynamics of lipid membrane interactions in the presence of zwitterionic buffers. *Biophys. J.* 101:362–369.
27. Gondré-Lewis, M. C., H. I. Petrache, …, Y. P. Loh. 2006. Abnormal sterols in cholesterol-deficiency diseases cause secretory granule malformation and decreased membrane curvature. *J. Cell Sci.* 119:1876–1885.
28. Karrer, H. E. 1958. The ultrastructure of mouse lung: the alveolar macrophage. *J. Biophys. Biochem. Cytol.* 4:693–700.
29. Hocking, W. G., and D. W. Golde. 1979. The pulmonary-alveolar macrophage (first of two parts). *N. Engl. J. Med.* 301:580–587.
30. Hocking, W. G., and D. W. Golde. 1979. The pulmonary-alveolar macrophage (second of two parts). *N. Engl. J. Med.* 301:639–645.
31. Hodge, S., G. Hodge, …, M. Holmes. 2003. Alveolar macrophages from subjects with chronic obstructive pulmonary disease are deficient in their ability to phagocytose apoptotic airway epithelial cells. *Immunol. Cell Biol.* 81:289–296.
32. Petrusca, D. N., Y. Gu, …, I. Petrache. 2010. Sphingolipid-mediated inhibition of apoptotic cell clearance by alveolar macrophages. *J. Biol. Chem.* 285:40322–40332.
33. Goñi, F. M., and A. Alonso. 2006. Biophysics of sphingolipids I. Membrane properties of sphingosine, ceramides and other simple sphingolipids. *Biochim. Biophys. Acta.* 1758:1902–1921.

34. de Jager, M. W., G. S. Gooris, …, J. A. Bouwstra. 2005. Lipid mixtures prepared with well-defined synthetic ceramides closely mimic the unique stratum corneum lipid phase behavior. *J. Lipid Res.* 46:2649–2656.

35. Janssens, M., J. van Smeden, …, J. A. Bouwstra. 2012. Increase in short-chain ceramides correlates with an altered lipid organization and decreased barrier function in atopic eczema patients. *J. Lipid Res.* 53:2755–2766.

36. Fenske, D. B., J. L. Thewalt, …, N. Kitson. 1994. Models of stratum corneum intercellular membranes: ^{2}H NMR of macroscopically oriented multilayers. *Biophys. J.* 67:1562–1573.

37. Okazaki, T., A. Bielawska, …, Y. A. Hannun. 1990. Role of ceramide as a lipid mediator of 1 α,25-dihydroxyvitamin D3-induced HL-60 cell differentiation. *J. Biol. Chem.* 265:15823–15831.

38. Venable, M. E., J. Y. Lee, …, L. M. Obeid. 1995. Role of ceramide in cellular senescence. *J. Biol. Chem.* 270:30701–30708.

39. Adan-Gokbulut, A., M. Kartal-Yandim, …, Y. Baran. 2013. Novel agents targeting bioactive sphingolipids for the treatment of cancer. *Curr. Med. Chem.* 20:108–122.

40. Petrache, I., V. Natarajan, …, R. M. Tuder. 2005. Ceramide upregulation causes pulmonary cell apoptosis and emphysema-like disease in mice. *Nat. Med.* 11:491–498.

41. Park, S. S., M. O. Kim, …, H. J. Han. 2013. C_{16}-ceramide-induced F-actin regulation stimulates mouse embryonic stem cell migration: involvement of N-WASP/Cdc42/Arp2/3 complex and cofilin-1/α-actinin. *Biochim. Biophys. Acta.* 1831:350–360.

42. McIntosh, T. J., M. E. Stewart, and D. T. Downing. 1996. X-ray diffraction analysis of isolated skin lipids: reconstitution of intercellular lipid domains. *Biochemistry.* 35:3649–3653.

43. McIntosh, T. J. 2003. Organization of skin stratum corneum extracellular lamellae: diffraction evidence for asymmetric distribution of cholesterol. *Biophys. J.* 85:1675–1681.

44. Holopainen, J. M., J. Lemmich, …, P. K. J. Kinnunen. 2000. Dimyristoylphosphatidylcholine/C16:0-ceramide binary liposomes studied by differential scanning calorimetry and wide- and small-angle x-ray scattering. *Biophys. J.* 78:2459–2469.

45. Holopainen, J. M., H. L. Brockman, …, P. K. J. Kinnunen. 2001. Interfacial interactions of ceramide with dimyristoylphosphatidylcholine: impact of the N-acyl chain. *Biophys. J.* 80:765–775.

46. Massey, J. B. 2001. Interaction of ceramides with phosphatidylcholine, sphingomyelin and sphingomyelin/cholesterol bilayers. *Biochim. Biophys. Acta.* 1510:167–184.

47. Sot, J., F. J. Aranda, …, A. Alonso. 2005. Different effects of long- and short-chain ceramides on the gel-fluid and lamellar-hexagonal transitions of phospholipids: a calorimetric, NMR, and x-ray diffraction study. *Biophys. J.* 88:3368–3380.

48. Westerlund, B., P.-M. Grandell, …, J. P. Slotte. 2010. Ceramide acyl chain length markedly influences miscibility with palmitoyl sphingomyelin in bilayer membranes. *Eur. Biophys. J.* 39:1117–1128.

49. Hsueh, Y.-W., R. Giles, …, J. Thewalt. 2002. The effect of ceramide on phosphatidylcholine membranes: a deuterium NMR study. *Biophys. J.* 82:3089–3095.

50. Goñi, F. M., and A. Alonso. 2009. Effects of ceramide and other simple sphingolipids on membrane lateral structure. *Biochim. Biophys. Acta.* 1788:169–177.

51. Silva, L. C., A. H. Futerman, and M. Prieto. 2009. Lipid raft composition modulates sphingomyelinase activity and ceramide-induced membrane physical alterations. *Biophys. J.* 96:3210–3222.

52. Wassall, S. R., and W. Stillwell. 2009. Polyunsaturated fatty acid-cholesterol interactions: domain formation in membranes. *Biochim. Biophys. Acta.* 1788:24–32.

53. Gulbins, E., and R. Kolesnick. 2003. Raft ceramide in molecular medicine. *Oncogene.* 22:7070–7077.

54. Soni, S. P., D. S. LoCascio, …, S. R. Wassall. 2008. Docosahexaenoic acid enhances segregation of lipids between raft and nonraft domains: ^{2}H NMR study. *Biophys. J.* 95:203–214.

55. Davis, J. H., K. R. Jeffrey, …, T. P. Higgs. 1976. Quadrupolar echo deuteron magnetic resonance spectroscopy in ordered hydrocarbon chains. *Chem. Phys. Lett.* 42:390–394.

56. Davis, J. H. 1983. The description of membrane lipid conformation, order and dynamics by ^{2}H-NMR. *Biochim. Biophys. Acta.* 737:117–171.

57. McCabe, M. A., and S. R. Wassall. 1997. Rapid deconvolution of NMR powder spectra by weighted fast Fourier transformation. *Solid State Nucl. Magn. Reson.* 10:53–61.

58. Lafleur, M., B. Fine, …, M. Bloom. 1989. Smoothed orientational order profile of lipid bilayers by ^{2}H-nuclear magnetic resonance. *Biophys. J.* 56:1037–1041.

59. Hed, J., G. Hallden, …, P. Larsson. 1987. The use of fluorescence quenching in flow cytofluorometry to measure the attachment and ingestion phases in phagocytosis in peripheral blood without prior cell separation. *J. Immunol. Methods.* 101:119–125.

60. Pérez, R., M. A. Balboa, and J. Balsinde. 2006. Involvement of group VIA calcium-independent phospholipase A2 in macrophage engulfment of hydrogen peroxide-treated U937 cells. *J. Immunol.* 176:2555–2561.

61. Deme, B., M. Dubois, …, T. Zemb. 2002. Giant collective fluctuations of charged membranes at the lamellar-to-vesicle unbinding transition. 1. Characterization of a new lipid morphology by SANS, SAXS, and electron microscopy. *Langmuir.* 18:997–1004.

62. Leibler, S., and R. Lipowsky. 1987. Complete unbinding and quasi-long-range order in lamellar phases. *Phys. Rev. B Condens. Matter.* 35:7004–7009.

63. Parsegian, V. A., and T. Zemb. 2011. Hydration forces: observations, explanations, expectations, questions. *Curr. Opin. Colloid Interface Sci.* 16:618–624.

64. Mccabe, M. A., and S. R. Wassall. 1995. Fast-Fourier-transform depaking. *J. Magn. Reson. B.* 106:80–82.

65. Huster, D., K. Arnold, and K. Gawrisch. 1998. Influence of docosahexaenoic acid and cholesterol on lateral lipid organization in phospholipid mixtures. *Biochemistry.* 37:17299–17308.

66. Seelig, J. 1977. Deuterium magnetic resonance: theory and application to lipid membranes. *Q. Rev. Biophys.* 10:353–418.

67. Petrache, H. I., and M. F. Brown. 2007. X-ray scattering and solid-state 2H NMR probes of structural fluctuations in lipid membranes. *Methods Mol. Biol.* 400:341–353.

68. Chernomordik, L. V., and M. M. Kozlov. 2008. Mechanics of membrane fusion. *Nat. Struct. Mol. Biol.* 15:675–683.

69. Seumois, G., M. Fillet, …, F. Bureau. 2007. De novo C16- and C24-ceramide generation contributes to spontaneous neutrophil apoptosis. *J. Leukoc. Biol.* 81:1477–1486.

70. Medler, T. R., D. N. Petrusca, …, I. Petrache. 2008. Apoptotic sphingolipid signaling by ceramides in lung endothelial cells. *Am. J. Respir. Cell Mol. Biol.* 38:639–646.

71. Heberle, F. A., J. Wu, …, G. W. Feigenson. 2010. Comparison of three ternary lipid bilayer mixtures: FRET and ESR reveal nanodomains. *Biophys. J.* 99:3309–3318.